Editors' Suggestion | Featured in Physics

Many-Body Description of STM-Induced Fluorescence of Charged Molecules

Song Jiang,[1,*] Tomáš Neuman,[2,†] Rémi Bretel,[2] Alex Boeglin,[1] Fabrice Scheurer,[1] Eric Le Moal,[2] and Guillaume Schull[1,‡]

[1]*Université de Strasbourg, CNRS, IPCMS, UMR 7504, F-67000 Strasbourg, France*

[2]*Institut des Sciences Moléculaires d'Orsay (ISMO), UMR 8214, CNRS, Université Paris-Saclay, 91405 Orsay Cedex, France*

(Received 7 October 2022; accepted 30 January 2023; published 21 March 2023)

A scanning tunneling microscope is used to study the fluorescence of a model charged molecule (quinacridone) adsorbed on a sodium chloride (NaCl)-covered metallic sample. Fluorescence from the neutral and positively charged species is reported and imaged using hyperresolved fluorescence microscopy. A many-body model is established based on a detailed analysis of voltage, current, and spatial dependences of the fluorescence and electron transport features. This model reveals that quinacridone adopts a palette of charge states, transient or not, depending on the voltage used and the nature of the underlying substrate. This model has a universal character and clarifies the transport and fluorescence mechanisms of molecules adsorbed on thin insulators.

DOI: 10.1103/PhysRevLett.130.126202

Fluorescence of neutral and charged molecules has been reported with subnanometer resolution in scanning tunneling microscopy induced-luminescence (STML) experiments over the last years [1–13]. In these experiments, charged emission is generally probed during transient charging of neutral molecules adsorbed on a thin decoupling layer [5,9,12]. STML of molecules whose ground state on surface is a negatively charged doublet (D_0^-) has also been reported for perylenetetracarboxylic dianhydride (PTCDA) in two recent works [6,13] where a low energy emission line was observed and assigned either to phosphorescence or to the emission of the negatively charged molecule. For PTCDA, deciphering which of those two emission channels is at play is tedious, especially because the transition dipole moments of the phosphorescence and negative trion are collinear, giving rise to similar patterns in STML maps.

Here, we report on a STML study of a model quinacridone (QA) molecule, whose ground state is a positively charged doublet (D_0^+) when adsorbed on four-monolayer (4 ML) NaCl/Ag(111). A rare property of this molecule is that neutral and positively charged fluorescence dipoles are oriented at ≈65° from each other, leading to distinct patterns in STML maps. This allows us to exclude phosphorescence and to assign the low energy emission line to the positive QA trion. Based on a comparison between the spatial, bias voltage, and tunneling current dependences of the charged and neutral emission, and on conductance data, a many-body description of the system [14–19] is set. It reveals that four different charged states of QA (QA^-, QA^0, QA^+, and QA^{2+}), involving three different spin multiplicities (singlet, doublet, triplet), can be populated within a single voltage sweep. This excitation mechanism is backed up by data obtained for QA deposited on NaCl/Au(111) where the ground state of the molecule is a doubly positively charged singlet state (S_0^{2+}). This model bears a universal character that can be applied to STML experiments dealing with charged and neutral molecules.

The data were acquired with a 4.5 K Omicron STM operating in ultrahigh vacuum adapted to detect the luminescence from the tip-sample junction (details in Supplemental Material [20]). Ag(111) and Au(111) substrates were cleaned with successive sputtering and annealing cycles. Electrochemically etched gold tips were introduced in the substrates to tune their plasmonic response. NaCl was thermally evaporated on the substrates kept at room temperature. The samples were then annealed to ∼430 K to obtain three to four-monolayer-thick NaCl films. QA molecules were thermally sublimated (at ∼560 K) onto the cold (∼4.5 K) substrate.

Figure 1(a) shows a sketch of the experiment, where the STM tip is used to excite the fluorescence of a QA molecule on 4 ML NaCl/Ag(111). In Fig. 1(b) one identifies individual molecules adsorbed on a NaCl cluster. Figure 1(c) provides a typical conductance spectrum (dI/dV) acquired on the decoupled QA, together with a close-up view of a molecule revealing its adsorption site on NaCl. Interestingly, the dI/dV spectrum shows two nearly symmetric resonances below (at a sample bias $V = -1.3$ V) and above ($V = 1.0$ V) the Fermi level, whose associated maps [Fig. 1(d)] reveal patterns strongly resembling the shape of the highest occupied molecular orbital (HOMO) calculated using density functional theory (DFT). This observation indicates that the ground state of the QA molecule is here the positively charged doublet (D_0^+) as indeed, in this configuration, adding or removing an electron from the molecule with the tip involves the

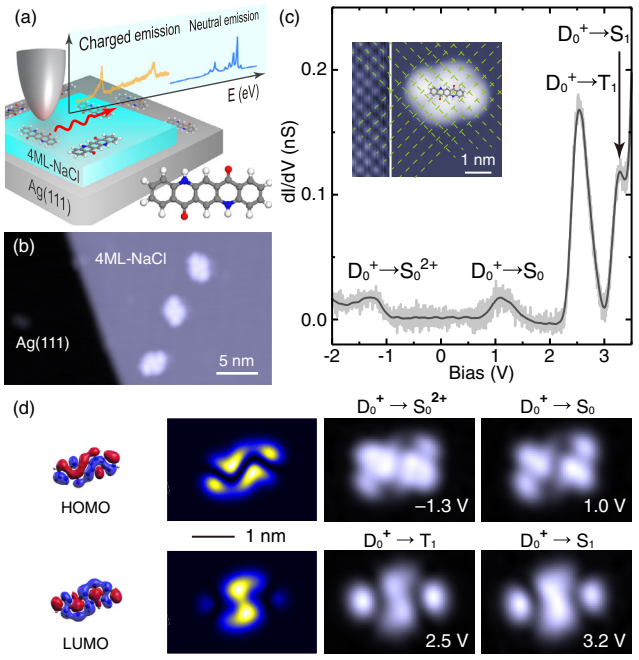

FIG. 1. (a) Sketch of the STML experiment on QA where neutral and charged fluorescence are represented. (b) STM image ($V = 2.8$ V, $I = 5$ pA) of QA molecules adsorbed on a 4 ML-NaCl island on Ag(111). (c) dI/dV spectrum recorded at the center of a QA molecule on 4 ML-NaCl. Inset: STM image of QA on 4 ML-NaCl/Ag(111) (left part: $V = 0.4$ V and $I = 500$ pA, and right part: $V = 2.6$ V and $I = 5$ pA). (d) DFT calculations (details in Supplemental Material [20]) of the frontier orbitals of the neutral molecule and corresponding maps of their partial density of states at constant height shown alongside with experimental dI/dV maps acquired at voltages corresponding to dI/dV resonances in (c).

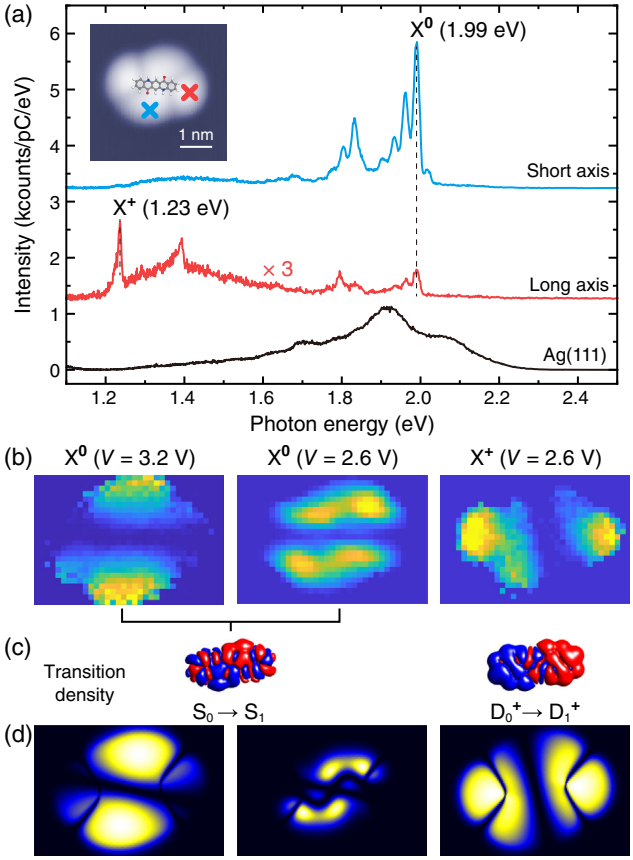

FIG. 2. (a) STML spectra acquired ($V = 2.7$ V, $I = 100$ pA, acquisition time $t = 300$ s) at the positions identified in the inset by crosses and reference spectrum acquired on Ag(111) ($V = 2.7$ V, $I = 200$ pA, $t = 30$ s). (b) HRFMs of QA on 4 ML-NaCl/Ag(111) for the neutral (X^0) and charged emission (X^+) (3.5 nm × 2.4 nm, $V = 2.6$ V, $t = 30$ s/pixel). (c) Transition electron density of $S_0 \rightarrow S_1$ and $D_0^+ \rightarrow D_1^+$ calculated using TDDFT. (d) Simulations of the HRFMs (see text for details).

HOMO of the molecule. Similar conclusions have been reported in previous works on decoupled molecules [6,32,33], where the two symmetric resonances are assigned to the singly occupied molecular orbital and unoccupied molecular orbital states in a single-particle picture. In our many-body description, the $V = -1.3$ V and $V = 1.0$ V resonances are associated with the $D_0^+ \rightarrow S_0^{2+}$ and $D_0^+ \rightarrow S_0$ transitions, respectively. In contrast, the maps associated with the two other dI/dV resonances observed at higher positive voltages ($V = 2.5$ V and $V = 3.2$ V) present patterns characteristic of the lowest unoccupied molecular orbital (LUMO). For reasons that will become clear later, we assign these two resonances to transitions to the triplet ($D_0^+ \rightarrow T_1$) and excited singlet ($D_0^+ \rightarrow S_1$) state of the neutral molecule. The resonance corresponding to the triplet state is more intense than the one associated to the excited singlet state, a phenomenon inherent to the larger triplet state spin multiplicity (details in Supplemental Material [20]). Molecular triplet states were inferred or directly measured in several scanning probe measurements recently [6,7,18,34]. Therefore, identifying triplet states as a resonance in the dI/dV spectra and clarifying its role in the luminescence spectra is crucial.

In Fig. 2(a) , we show STML spectra (blue and red lines) acquired at $V = 2.7$ V for two different positions of the tip on the molecule (blue and red crosses) corresponding to excitations along the short and long axes of QA, together with a reference spectrum acquired on Ag(111) (in black). The blue spectrum reveals an emission line at a photon energy $h\nu = 1.99$ eV (labeled X^0) followed, on its lower-energy side, by a series of vibronic lines, which fits the emission of neutral QA ($S_1 \rightarrow S_0$) well. The same contribution is identified in the red spectrum with a weaker intensity. It is accompanied by two lower-energy lines at $h\nu = 1.23$ eV (labeled X^+) and $h\nu = 1.39$ eV, whose identification cannot rely only on literature.

In Fig. 2(b) we display hyperresolved fluorescence maps (HRFMs) of the emission intensity of X^0 (recorded at $V = 3.2$ V and $V = 2.6$ V) and of X^+ (recorded at $V = 2.6$ V). The HRFMs exhibit two bright features separated by a

nearly horizontal (X^0) or vertical (X^+) node. It has been demonstrated [2,17,35,36] that the axis joining the two bright lobes in the HRFMs provides the orientation of the exciton transition dipole moment. For X^0, the dipole axis is tilted horizontally by ≈65° with respect to the long axis of QA, as shown also by the $S_1 \rightarrow S_0$ transition simulated using time-dependent density-functional theory (TDDFT) in Fig. 2(c) (details in Supplemental Material [20]). The same orientation holds for the dipole associated to the phosphorescence $T_1 \rightarrow S_0$. In contrast, the HRFM of X^+ reveals a transition dipole moment nearly parallel to the long QA axis. This behavior agrees with TDDFT simulations [Fig. 2(c)] of the positively charged QA trion (X^+) corresponding to a $D_1^+ \rightarrow D_0^+$ radiative transition. For the emission line at 1.39 eV, the HRFM reveals a pattern similar to the one for X^+ (see Supplemental Material [20]). Together with spectra recorded in the short-wave infrared range (see Supplemental Material [20]), these data associate the 1.39 eV line to the luminescence from a nonrelaxed vibronic state of D_1^+. Eventually, the X^0 HRFMs recorded at $V = 3.2$ V and $V = 2.6$ V reveal two slightly different patterns, reflecting different excitation mechanisms as is accounted for in the theoretical model described below and in Fig. 2(d).

To support our assignment of the spectral contributions and to determine the excitation mechanism leading to the emission of the charged and neutral QA molecule, we recorded the voltage [Fig. 3(a)] and current [Figs. 3(b) and 3(c)] dependences of X^0 and X^+. Figure 3(a) shows that the emission onset of X^+ coincides with resonant electron tunneling into the triplet state ($D_0^+ \rightarrow T_1$). Besides, the X^+ emission intensity varies linearly with current [Figs. 3(b) and 3(c)], indicating a single electron excitation process. Based on these observations we build a robust many-body scheme [Fig. 3(d)] to explain the X^+ emission. The molecule initially in the ground D_0^+ state can be driven, for $V > 2.3$ V, into T_1 by injection of an electron from the tip into the LUMO of the molecule. The molecule can return to its cationic state by electron tunneling to the substrate either from the LUMO ($T_1 \rightarrow D_0^+$) or from the HOMO, thus populating a higher excited state D_n^+ ($T_1 \rightarrow D_n^+$) [37]. In the latter case, the trionic excited state D_n^+ rapidly decays to D_1^+. The radiative transition ($D_1^+ \rightarrow D_0^+$) is eventually responsible for the X^+ emission line (as confirmed by TDDFT in Supplemental Material [20]). The only condition for this mechanism to occur is that T_1 has a higher energy than D_n^+ in Fig. 3(d). According to the sketch shown in Fig. 3(d), one may also expect phosphorescence ($T_1 \rightarrow S_0$) at ≈1.6 eV. Phosphorescence is, however, a very slow process in comparison with the $T_1 \rightarrow D_n^+$ transition (in the nanosecond range according to [38]). Phosphorescence is therefore quenched by charge transfer from the substrate, explaining its absence in our STML spectra.

The situation is more complex for X^0. The voltage dependence in Fig. 3(a) reveals two emission onsets at

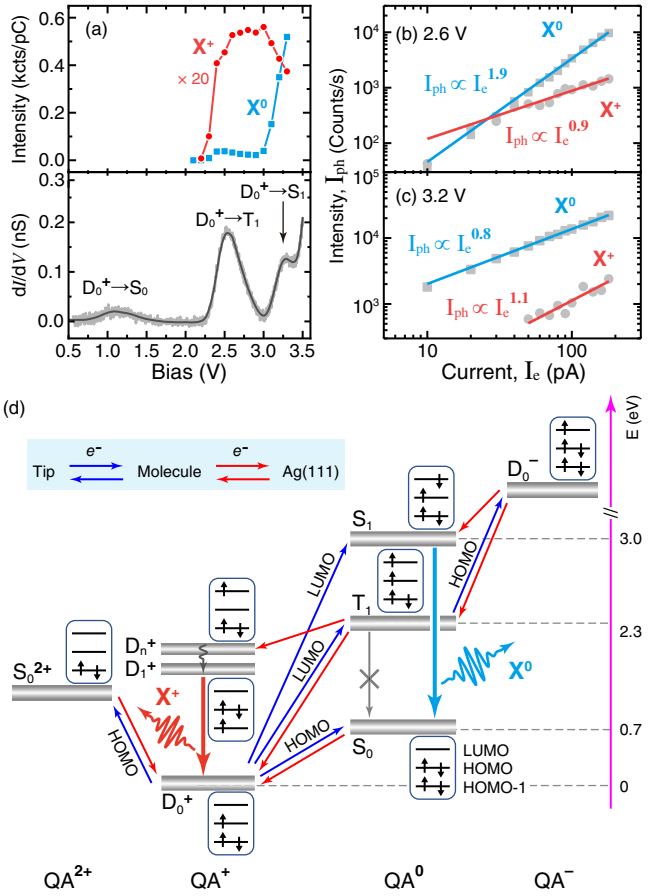

FIG. 3. (a) Voltage dependences of the neutral (X^0, blue squares) and charged (X^+, red circles) emission intensities measured at a constant current ($I = 50$ pA) and dI/dV spectrum of a QA/NaCl(4 ML)/Ag(111) (bottom panel). Current dependences of the neutral (X^0, blue squares) and charged (X^+, red dots) emission intensities measured at (b) $V = 2.6$ V and (c) $V = 3.2$ V. (d) Sketches of the luminescence mechanisms for the neutral and charged QA emission.

$V = 2.4$ V and $V = 3.0$ V, respectively. The first onset leads to a weak X^0 emission and coincides with the $D_0^+ \rightarrow T_1$ transition in the dI/dV spectrum. The second onset leads to a comparatively much brighter emission and corresponds to the ($D_0^+ \rightarrow S_1$) transition. Figure 3(b) reveals a nearly quadratic dependence of the X^0 intensity on the tunneling current for voltages corresponding to the first onset, indicating a two-electron excitation mechanism. In contrast, the linear current dependence of the X^0 emission after the second onset [Fig. 3(c)] indicates a one-electron process at this voltage.

The intense emission of X^0 for $V > 3.0$ V finds its origin in the fact that one can directly populate the excited singlet state S_1 of the molecule, which in turn rapidly decays in the neutral ground state S_0 by emitting an X^0 photon. For 2.3 V $< V <$ 3.0 V, only T_1 is populated. As T_1 is a long-lived triplet state, a second tunneling event from the tip can take place, driving the QA molecule in the negatively

charged doublet state D_0^-. From there, the tunneling of an electron from the HOMO to the sample can drive the molecule into the S_1 state, where radiative recombination to S_0 may occur. In contrast to the other many-body states discussed so far that are all directly observed either in conductance or fluorescence spectra, the presence of the D_0^- state can, in principle, only be inferred from the current and voltage dependences of the X^0 line. However, some information about this two-electron excitation mechanism can also be deduced from the difference between the X^0 line HRFMs recorded at $V = 3.2$ V and $V = 2.6$ V [Figs. 2(b)–2(d)]. Whereas the first one can be well reproduced by considering a simple charge transfer from the tip to the LUMO of the molecule (reflecting the $D_0^+ \rightarrow S_1$ transition), the second involves the LUMO ($D_0^+ \rightarrow T_1$ transition) and the HOMO ($T_1 \rightarrow D_0^-$ transition).

This can be accounted for in a theoretical rate-equation model where the input rates of all tip-mediated processes—electron tunneling and photon emission—are made tip-position-dependent (details in Supplemental Material [20]). The tip-mediated tunneling rates [blue arrows in Fig. 3(d)] are considered proportional to the relevant partial density of states [14,39] and the plasmon-mediated photon emission [thick vertical arrows in Fig. 3(d)] is included by evaluating the plasmon-exciton coupling strength [36]. We solve the rate equations in the steady state for a given voltage at each position of the tip and thus extract the HRFMs. The calculated maps, shown in Fig. 2(d), are in excellent agreement with the experiment, demonstrating that, beyond the information related to the plasmon-exciton coupling, the patterns of the HRFMs can be used to identify the role of specific molecular many-body states in the STML excitation mechanism.

To further confirm and extend our understanding of the excitation mechanism, we performed a similar experiment with QA adsorbed on 3 ML NaCl/Au(111), as shown in Fig. 4(a). The work function of Au(111) is about 0.8 eV higher than that of Ag(111), which causes a shift of the molecular states to higher energies, and eventually leads to an adsorbed molecule in a doubly charged singlet state S_0^{2+}. This unusual electronic configuration can be visualized in Fig. 4(b) where the dI/dV spectrum reveals three spectroscopic features assigned to transitions to the triply charged doublet state D_0^{3+} ($V = -3$ V), the doublet state D_0^+ ($V = 1$ V) and the excited doublet state D_n^+ ($V = 2.5$ V), respectively [37]. STML spectra and HRFM reveal [Fig. 4(d)] the characteristic features of the X^+ emission. The X^0 emission is absent, independently of the used voltage, current, and tip position conditions. Indeed, as the molecule is initially in a doubly charged state, populating S_1, a mandatory step for the X^0 emission, would rely on an inefficient two-electron process and require a very high voltage to enable the $D_0^+ \rightarrow S_1$ transition. The X^+ voltage onset [$V \approx 2.3$ V, see Fig. 4(b)] correlates well with the

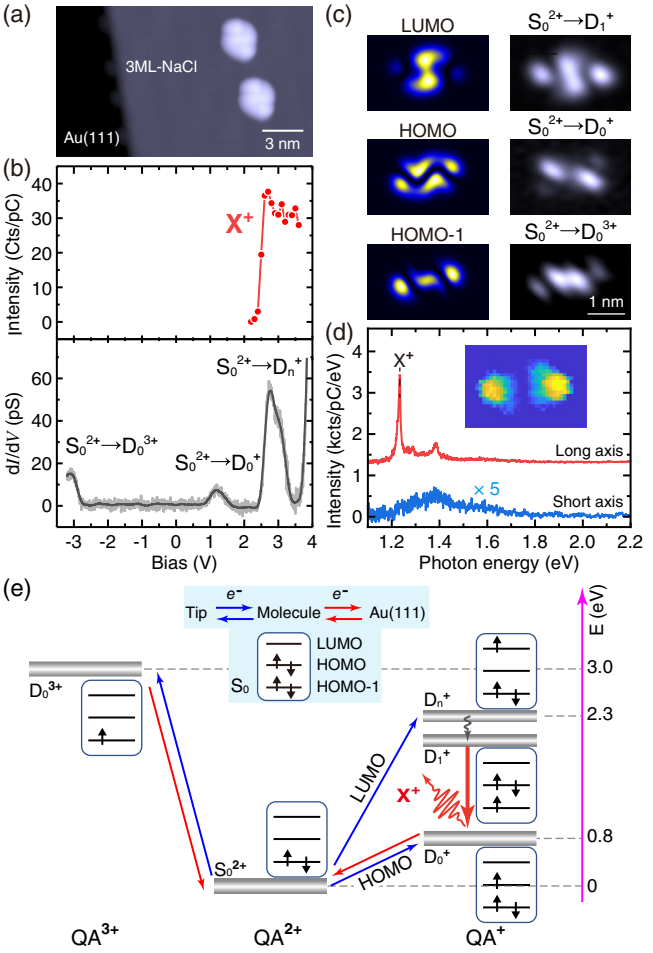

FIG. 4. (a) STM image ($V = 2.9$ V, $I = 5$ pA) of QA adsorbed on a 3 ML-NaCl/Au(111). (b) Voltage dependence of the X^+ emission (top) and dI/dV spectrum (bottom) recorded for QA/NaCl(3 ML)/Au(111). (c) DFT simulations of the partial density of states derived from the LUMO, HOMO, and HOMO-1 of the neutral QA evaluated at a constant height above the molecule (left), and constant height dI/dV maps (right) acquired at voltages corresponding to the resonances in the dI/dV in (b). (d) STML spectra acquired ($V = 2.9$ V, $I = 50$ pA, $t = 180$ s) at the short and long axis of the molecule. Inset: HRFM of X^+ for QA on 3 ML-NaCl/Au(111) (3.5 nm × 2.4 nm, $V = 2.9$ V, $t = 30$ s/pixel.) (e) Sketch of the luminescence mechanisms for QA on 3 ML-NaCl/Au(111).

$S_0^{2+} \rightarrow D_n^+$ transition, and suggests a nonradiative $D_n^+ \rightarrow D_1^+$ transition.

On the basis of these observations one can therefore establish the many-body state diagram shown in Fig. 4(e). This diagram perfectly explains that the constant height dI/dV maps [Fig. 4(c)] show patterns corresponding (i) to the LUMO for the resonance corresponding to the $S_0^{2+} \rightarrow D_n^+$ transition, (ii) to the HOMO for the resonance corresponding to the $S_0^{2+} \rightarrow D_0^+$, and (iii) to the HOMO-1 for the resonance corresponding to the $S_0^{2+} \rightarrow D_0^{3+}$ transition. Note that, in this last case, the molecule is transiently driven in an unexpected triply charged state. Eventually, we want to

stress that our representation could be further improved by accounting for molecular vibrations and substrate reorganizations that are known to play an important role in the energy of the allowed electronic transitions [40,41].

Overall, we report on STML measurements of a model system for charged molecules. Our study demonstrates that the emission line strongly redshifted with respect to the neutral fluorescence should be assigned to trionic emission. Our Letter also provides a very consistent picture based on current, voltage and spatial dependences of STML signals as well as on conductance spectra and maps for the same molecule on two different substrates. This shows that four different charged states of a molecule, involving three different spin multiplicities, can be populated during a single voltage sweep. This also allows establishing a solid many-body model explaining in details the transport and light emission mechanisms, which can readily be applied to other STML experiments dealing with decoupled molecules or more complex emitters.

We thank Niklas Humberg and Moritz Sokolowski for drawing our attention to the quinacridone molecule and for providing it. Anna Rosławska, Katharina Kaiser, and Kirill Vasilev are acknowledged for discussions. We are grateful to Virginie Speisser and Michelangelo Romeo for technical support. This project has received funding from the European Research Council (ERC) under the European Union's Horizon 2020 research and innovation program (Grant Agreement No. 771850). The International Center for Frontier Research in Chemistry (FRC) is acknowledged for financial support. This work has been supported by the University of Strasbourg's IdEx program and by the "Investissements d'Avenir" LabEx PALM (ANR-10-LABX-0039-PALM) and the ANR (ANR-16-CE24-0003).

*song.jiang@ipcms.unistra.fr
†neuman@fzu.cz
‡guillaume.schull@ipcms.unistra.fr

[1] X. Qiu, G. Nazin, and W. Ho, Science **299**, 542 (2003).
[2] Y. Zhang, Y. Luo, Y. Zhang, Y.-J. Yu, Y.-M. Kuang, L. Zhang, Q.-S. Meng, Y. Luo, J.-L. Yang, Z.-C. Dong *et al.*, Nature (London) **531**, 623 (2016).
[3] H. Imada, K. Miwa, M. Imai-Imada, S. Kawahara, K. Kimura, and Y. Kim, Nature (London) **538**, 364 (2016).
[4] B. Doppagne, M. C. Chong, E. Lorchat, S. Berciaud, M. Romeo, H. Bulou, A. Boeglin, F. Scheurer, and G. Schull, Phys. Rev. Lett. **118**, 127401 (2017).
[5] B. Doppagne, M. C. Chong, H. Bulou, A. Boeglin, F. Scheurer, and G. Schull, Science **361**, 251 (2018).
[6] K. Kimura, K. Miwa, H. Imada, M. Imai-Imada, S. Kawahara, J. Takeya, M. Kawai, M. Galperin, and Y. Kim, Nature (London) **570**, 210 (2019).
[7] G. Chen, Y. Luo, H. Gao, J. Jiang, Y. Yu, L. Zhang, Y. Zhang, X. Li, Z. Zhang, and Z. Dong, Phys. Rev. Lett. **122**, 177401 (2019).
[8] K. Kaiser, L. Gross, and F. Schulz, ACS Nano **13**, 6947 (2019).
[9] V. Rai, L. Gerhard, Q. Sun, C. Holzer, T. Repän, M. Krstić, L. Yang, M. Wegener, C. Rockstuhl, and W. Wulfhekel, Nano Lett. **20**, 7600 (2020).
[10] F.-F. Kong, X.-J. Tian, Y. Zhang, Y.-J. Yu, S.-H. Jing, Y. Zhang, G.-J. Tian, Y. Luo, J.-L. Yang, Z.-C. Dong *et al.*, Nat. Commun. **12**, 1280 (2021).
[11] T.-C. Hung, B. Kiraly, J. H. Strik, A. A. Khajetoorians, and D. Wegner, Nano Lett. **21**, 5006 (2021).
[12] J. Dolezal, S. Canola, P. Merino, and M. Svec, ACS Nano **15**, 7694 (2021).
[13] J. Dolezal, S. Canola, P. Hapala, R. C. de Campos Ferreira, P. Merino, and M. Svec, ACS Nano **16**, 1082 (2021).
[14] F. Schulz, M. Ijäs, R. Drost, S. K. Hämäläinen, A. Harju, A. P. Seitsonen, and P. Liljeroth, Nat. Phys. **11**, 229 (2015).
[15] P. Yu, N. Kocić, J. Repp, B. Siegert, and A. Donarini, Phys. Rev. Lett. **119**, 056801 (2017).
[16] K. Miwa, H. Imada, M. Imai-Imada, K. Kimura, M. Galperin, and Y. Kim, Nano Lett. **19**, 2803 (2019).
[17] B. Doppagne, T. Neuman, R. Soria-Martinez, L. E. P. López, H. Bulou, M. Romeo, S. Berciaud, F. Scheurer, J. Aizpurua, and G. Schull, Nat. Nanotechnol. **15**, 207 (2020).
[18] S. Fatayer, F. Albrecht, I. Tavernelli, M. Persson, N. Moll, and L. Gross, Phys. Rev. Lett. **126**, 176801 (2021).
[19] S. Jiang, T. Neuman, A. Boeglin, F. Scheurer, and G. Schull, Science **379**, 1049 (2023).
[20] See Supplemental Material at http://link.aps.org/supplemental/10.1103/PhysRevLett.130.126202, which includes Refs. [21–31], for additional experimental methods and experimental data and more detailed discussion on theoretical modeling.
[21] M. C. Chong, G. Reecht, H. Bulou, A. Boeglin, F. Scheurer, F. Mathevet, and G. Schull, Phys. Rev. Lett. **116**, 036802 (2016).
[22] M. A. Baldo, D. F. O'Brien, M. E. Thompson, and S. R. Forrest, Phys. Rev. B **60**, 14422 (1999).
[23] H.-C. Ploigt, C. Brun, M. Pivetta, F. Patthey, and W.-D. Schneider, Phys. Rev. B **76**, 195404 (2007).
[24] F. Santoro, A. Lami, R. Improta, J. Bloino, and V. Barone, J. Chem. Phys. **128**, 224311 (2008).
[25] N. Tancogne-Dejean *et al.*, J. Chem. Phys. **152**, 124119 (2020).
[26] M. J. Frisch *et al.*, Gaussian 16 Revision C.01, 2016, Gaussian Inc. Wallingford CT.
[27] A. D. Becke, J. Chem. Phys. **98**, 5648 (1993).
[28] B. Champagne, V. Liégeois, and F. Zutterman, Photochem. Photobiol. Sci. **14**, 444 (2015).
[29] J. P. Perdew and A. Zunger, Phys. Rev. B **23**, 5048 (1981).
[30] P. A. M. Dirac, Math. Proc. Cambridge Philos. Soc. **26**, 376 (1930).
[31] J. Slater, Phys. Rev. **81**, 385 (1951).
[32] J. Repp, G. Meyer, S. Paavilainen, F. E. Olsson, and M. Persson, Science **312**, 1196 (2006).
[33] M. Hollerer, D. Lüftner, P. Hurdax, T. Ules, S. Soubatch, F. S. Tautz, G. Koller, P. Puschnig, M. Sterrer, and M. G. Ramsey, ACS Nano **11**, 6252 (2017).
[34] J. Peng, S. Sokolov, D. Hernangómez-Pérez, F. Evers, L. Gross, J. M. Lupton, and J. Repp, Science **373**, 452 (2021).

[35] C. Chen, P. Chu, C. A. Bobisch, D. L. Mills, and W. Ho, Phys. Rev. Lett. **105**, 217402 (2010).
[36] A. Rosławska, T. Neuman, B. Doppagne, A. G. Borisov, M. Romeo, F. Scheurer, J. Aizpurua, and G. Schull, Phys. Rev. X **12**, 011012 (2022).
[37] A direct transition to D_1^+ is unlikely as it would require a change of electronic configuration involving two different electrons and would not account for the LUMO pattern in the $S_0^{2+} \rightarrow D_n^+$ image in Fig. 4(c).
[38] K. Kaiser, L. A. Lieske, J. Repp, and L. Gross, arXiv: 2211.01051.
[39] J. Tersoff and D. R. Hamann, Phys. Rev. B **31**, 805 (1985).
[40] S. Fatayer, B. Schuler, W. Steurer, I. Scivetti, J. Repp, L. Gross, M. Persson, and G. Meyer, Nat. Nanotechnol. **13**, 376 (2018).
[41] D. Hernangómez-Pérez, J. Schlör, D. A. Egger, L. L. Patera, J. Repp, and F. Evers, Phys. Rev. B **102**, 115419 (2020).